

---

# AMLGENTEX: Mobilizing Data-Driven Research to Combat Money Laundering

---

**Johan Östman**  
AI Sweden

**Edvin Callisen**  
AI Sweden

**Anton Chen**  
Handelsbanken

**Kristiina Ausmees**  
Handelsbanken

**Emanuel Gårdh**  
Handelsbanken

**Jovan Zamac**  
Handelsbanken

**Jolanta Goldstein**  
Swedbank

**Hugo Wefer**  
Swedbank

**Simon Whelan**  
Swedbank

**Markus Reimegård**  
Swedbank

## Abstract

Money laundering enables organized crime by allowing illicit funds to enter the legitimate economy. Although trillions of dollars are laundered each year, only a small fraction is ever uncovered. This stems from a range of factors, including deliberate evasion by launderers, the rarity of confirmed cases, and the limited visibility each financial institution has into the global transaction network. While several synthetic datasets are available, they fail to model the structural and behavioral complexity of real-world money laundering. In particular, they often overlook partial observability, sparse and uncertain labels, strategic behavior, temporal dynamics, class imbalance, and network-level dependencies. To address these limitations, we present AMLGENTEX, an open-source suite for generating realistic, configurable transaction data and benchmarking detection methods. It enables systematic evaluation of anti-money laundering (AML) systems in a controlled environment that captures key real-world challenges. We demonstrate how the framework can be used to rigorously evaluate methods under conditions that reflect the complexity of practical AML scenarios.

## 1 Introduction

Money laundering is a critical enabler of organized crime, allowing illicit profits to be integrated into the legitimate economy [1, 2]. The scale of the problem is staggering: an estimated \$3.1 trillion in illicit funds flowed through the global financial system in 2023 alone [3], nearly doubling the \$1.6 trillion estimated in 2009 [4].

Global anti-money laundering (AML) efforts are anchored in the 2012 FATF Recommendations, which provide a comprehensive framework covering customer due diligence (CDD), including know-your-customer (KYC) procedures, risk profiling, transaction monitoring, reporting through Suspicious Activity Reports (SARs), and record-keeping requirements [5]. However, these recommendations do not prescribe specific implementations, leading to significant variation in how financial institutions (FIs) design risk strategies, CDD processes, and monitoring systems. In practice, most monitoring systems are rule-based.

Criminals frequently employ sophisticated tactics and rapidly adopt new technologies, often outpacing law enforcement [2]. They exploit structural weaknesses, such as the fact that FIs can only observe their internal transaction networks and that data sharing between institutions remains limited [3, 6]. As a result, AML efforts remain largely ineffective, with success rates estimated as low as 0.2% [7]. Compounding these difficulties is the scarcity of open, realistic AML datasets, which significantly hampers research and limits the development and benchmarking of better monitoring systems.

Beyond data limitations, several fundamental factors further amplify the inherent difficulty of AML detection. Based on expert assessments, we identify at least seven key challenges: (i) **Interdependencies**, since accounts are embedded in a global transaction network that must be considered during monitoring; (ii) **Imbalanced data**, as laundering events are extremely rare compared to legitimate transactions; (iii) **Privacy constraints**, limiting collaboration between institutions [3]; (iv) **Weak supervision**, due to the scarcity of ground-truth labels and the noisy nature of SARs, which often contain unverified or subjective suspicions rather than confirmed illicit activity; (v) **Temporal drift**, as transaction networks naturally evolve over time; (vi) **Adaptive adversaries**, where criminals actively change strategies to evade detection [8]; and (vii) **Heterophily**, as launderers deliberately mimic normal behavior, complicating graph-based methods. These challenges, along with their assessed severity, are visualized in Fig. 1.

In this work, we present a data-generation and benchmarking suite called AMLGENTEX<sup>1</sup>. Our contributions are threefold. First, we introduce an agent-based simulator combined with an optimization framework for generating transaction networks that capture all of the above challenges. The optimization can be performed in two modes, depending on the availability of external data. Second, because transaction networks are often difficult to oversee, we provide a visualization tool for seamless inspection and analysis of the generated data. Finally, AMLGENTEX includes a benchmarking suite that incorporates both traditional rule-based methods and recent graph-based detection techniques. We hope our work will facilitate research on AML by providing a foundation for creating more realistic and challenging datasets. AMLGENTEX also benefits practitioners by providing a controlled environment to develop and test monitoring systems with ground-truth labels.

## 2 Related Work

Several efforts have been made to synthetically replicate real-world transactional data for AML research. One of the earliest attempts was introduced by Lopez-Rojas and Axelsson [9], where the authors proposed a purely algorithmic multi-agent simulation focused on mobile payments. Agents probabilistically transitioned between fraudulent and benign behaviors without using any real data. This approach was extended in PAYSIM [10], which introduced a reference dataset to empirically estimate agent behavior. However, both works lack spatial structure, as transactions are generated independently across accounts. Moreover, PAYSIM requires an existing real-world dataset to calibrate parameters, which is often unavailable.

To address the lack of spatial components, IBM introduced AMLSIM [11], a multi-agent simulation that does not require a reference dataset. AMLSIM simulates transaction networks based on known AML typologies, categorized into normal and alert patterns. The normal patterns (e.g., direct, mutual, periodic, forward, fan-in, fan-out) and alert patterns (e.g., fan-in, fan-out, cycle, scatter-gather, gather-scatter) reflect typical and suspicious behaviors, respectively. Fig. 8 and Fig. 9 in App. A illustrate these structures. Notably, patterns such as fan-in and fan-out appear in both normal and alert categories, emphasizing how criminals often mimic legitimate activity.

The process of money laundering is often described as consisting of three stages: *placement*, *layering*, and *integration* [1, 2]. AMLSIM primarily focuses on the layering phase. Moreover, it models the transaction network as a closed system with no external inflow or outflow of funds, exhibits inconsistencies between specified and realized patterns, and supports only three of the aforementioned money laundering typologies. Recent efforts, such as [12], have sought to address the latter limitation by expanding the set of normal and alert patterns.

Altman et al. [13] proposed AMLWORLD, a framework that models relationships between individuals and companies using a circular flow graph. AMLWORLD explicitly simulates the placement, layering,

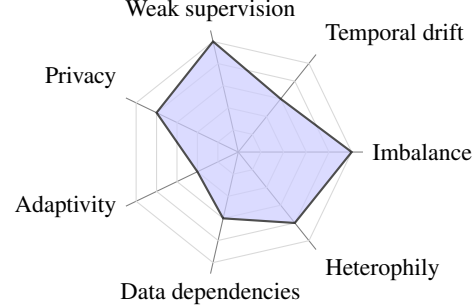


Figure 1: Assessed severity (0–5) of key challenges in transaction monitoring, based on expert opinions from AML practitioners.

<sup>1</sup> AMLGENTEX is open-source and available at <https://github.com/aidotse/AMLGentex>

and integration phases. Although the framework itself is not publicly available, the authors have released six datasets with varying ratios of alert transactions. However, as mentioned by the authors, the data generation demands extensive parameter tuning and it is unclear how this procedure was performed for the released datasets.

Project Aurora, an initiative by the Bank for International Settlements [6], explores the use of privacy-enhancing technologies (PETs) in AML through two months of synthetic transactions generated across six countries and 29 FIs. Although the data generation process is not disclosed, it follows principles similar to those underlying AMLSIM and AMLWORLD.

Beyond agent-based simulations, some approaches generate synthetic AML data using statistical models. For instance, SYNTHAML [14] uses Gaussian copulas to produce a synthetic dataset tuned on real transaction data from the Danish bank Spar Nord. The released dataset contains 440,000 clients, 16 million transactions, and 20,000 alert events, and captures entity behaviors such as repeated involvement in money laundering activities.

### 3 Preliminaries

We model the global transaction network at each time  $t \in [T]$  as a directed multigraph  $\mathcal{G}_t = (\mathcal{V}_t, \mathcal{E}_t, \tilde{\mathcal{X}}_t, \tilde{\mathbf{Y}}_t)$ . Here,  $\mathcal{V}_t$  denotes the set of active accounts at time  $t$ , where node indices are persistent across time. The multiset of edges is represented as  $\mathcal{E}_t = \{(u_i, v_i, a_i)\}_{i=1}^{|\mathcal{E}_t|}$ , where each transaction  $(u_i, v_i, a_i)$  corresponds to a directed transaction from account  $u_i$  to account  $v_i$  with associated attributes  $a_i \in \mathcal{A}$ , such as transaction amount, timestamp, or transaction type. The matrix  $\tilde{\mathbf{X}}_t \in \mathcal{X}_{\text{CDD}}^{|\mathcal{V}_t|}$  contains feature vectors associated with each account, where  $\mathcal{X}$  denotes the input space derived from the CDD process. Moreover, each transaction  $(u_i, v_i, a_i)$  is associated with a binary label  $\tilde{y}_i \in \{0, 1\}$  indicating whether the transaction is related to money laundering, and we denote the collection of all labels by  $\tilde{\mathbf{Y}}_t = \{y_i\}_{i=1}^{|\mathcal{E}_t|}$ .

Let  $w \subseteq [T]$  denote a consecutive window and let  $\text{AGG}(w) : \{\mathcal{G}_t\}_{t \in w} \rightarrow \mathcal{G}$  be an aggregation operator that combines the graphs over the window  $w$  into a single graph  $\mathcal{G} = (\mathcal{V}, \mathcal{E}, \mathbf{X}, \mathbf{Y})$  amenable to node classification. The aggregation proceeds as follows: the node set is given by the union  $\mathcal{V} = \bigcup_{t \in w} \mathcal{V}_t$ , and the edge set by the union  $\mathcal{E} = \bigcup_{t \in w} \mathcal{E}_t$ . For each node  $v \in \mathcal{V}$ , we construct a feature vector  $\mathbf{x}_v$  by concatenating its static CDD features with aggregated transaction-based features over  $w$ . The static features are taken from the latest time at which  $v$  appears, while the transaction-derived features may include metrics such as total in- and out-flux of funds and the number of unique counterparties. Formally,  $\mathbf{x}_v \in \mathcal{X}_{\text{CDD}} \times \mathcal{X}_{\text{TXN}}$ , where  $\mathcal{X}_{\text{TXN}}$  denotes the space of features derived from transactional activity over the aggregation window. For each node  $v \in \mathcal{V}$ , we define the node label  $y_v \in \{0, 1\}$  as

$$y_v = \mathbf{1}(\exists(u, v, a) \in \mathcal{E} \text{ or } (v, u, a) \in \mathcal{E} \text{ such that } \tilde{y}_{(u, v, a)} = 1 \text{ or } \tilde{y}_{(v, u, a)} = 1),$$

where  $\mathbf{1}(\cdot)$  denotes the indicator function.

### 4 Data Generation

The data generation process in AMLGENTEX builds on the multi-agent simulation framework AMLSIM, which we extend by: (i) introducing generalized typologies; (ii) modeling all three stages of money laundering through new placement and integration mechanisms [2]; (iii) simulating income and spending beyond a closed network; (iv) enabling control over transaction graph degree distributions; (v) supporting various types of label noise; (vi) incorporating external data sources such as demographic data [15] and transaction statistics [16]; and (vii) applying systematic hyperparameter tuning to improve data fidelity. We outline the process below.

#### 4.1 Account Relations

AMLGENTEX initiates by generating a **blueprint network**, where both the number of accounts and their in-degree and out-degree distributions are specified by the user. The distributions follow a scale free pattern, where most accounts have few connections and a small number have many, a structure

commonly observed in financial transaction networks [17]. The in- and out-degree distributions are realized via a discretized Pareto distribution

$$\mathbb{P}[\deg_u = k] = \frac{1}{\left(\frac{k-\text{loc}}{\text{scale}} + 1\right)^\gamma} - \frac{1}{\left(\frac{k-\text{loc}}{\text{scale}} + 2\right)^\gamma}, \quad k \geq \text{loc}, \quad \gamma > 0$$

with user-provided parameters  $\text{loc}$ ,  $\text{scale}$ , and  $\gamma$  controlling the minimum number of connections, spread, and slope of the distribution. The resulting degree distributions for various parameter configurations are illustrated in Fig. 10 of Appendix B.

Next, the blueprint network is populated with user defined typologies from both normal and money laundering scenarios (see Appendix A), based on user-specified number, size, and type, as far as possible. Notably, normal patterns are only included if they can be fully accommodated by the blueprint network, while money laundering patterns are injected regardless of fit.

Initially, no account is involved in money laundering and accounts are selected uniformly at random. As typologies are assigned, accounts are grouped according to how many money laundering patterns they have previously participated in. When assigning accounts to new money laundering patterns, at each selection step, with probability  $p$ , an account is selected from a group with prior participation rather than from the unused pool. Among the participating groups, selection proceeds recursively: with probability  $p$ , the process moves to a group with a higher participation count, continuing in this way until a group is chosen or the process stops with probability  $1 - p$ . This mechanism is inspired by real money laundering statistics [14, Fig. 1], where some accounts appear in multiple patterns. The number of money laundering patterns a malicious account participates in,  $n_{\text{ml}}$ , is modeled by a logarithmic distribution

$$\mathbb{P}[n_{\text{ml}} = k] = \frac{-1}{\log(1-p)} \cdot \frac{p^k}{k}$$

where  $p \in (0, 1)$  is a user defined parameter that controls the probability of reusing accounts. The resulting cumulative distribution function is shown in Appendix B, Fig. 11, for different values of  $p$ .

Since normal patterns must fit within the blueprint network, some patterns may be discarded depending on the input configuration. Likewise, due to the random assignments, some accounts may not participate in any pattern after the normal and alert patterns have been applied. These accounts are pruned from the transaction network, which ultimately alters the degree distribution of the resulting network. As a result, the targeted degree distribution may differ from the final degree distribution. The process of creating the relational network is illustrated in App. B, Fig. 12.

## 4.2 Account Interactions

With the account relationships established, the next step is to generate the transactions within each pattern. This is governed by a timing scheme, controlled by user provided start and end times. AMLGENTEX supports several timing schemes: fixed interval, random interval, unordered, and simultaneous. In the fixed interval scheme, transactions occur at regular, user defined intervals. In the random interval scheme, transaction times are sampled within a given time window. The unordered scheme allows transactions to occur at arbitrary times, while in the simultaneous scheme, all transactions within the pattern occur at the same time step. Some typologies also enforce a partial order on transactions. In forward and cycle patterns, transactions follow a strict sequential order. In scatter-gather, gather-scatter, and stacked bipartite patterns, transactions are randomly ordered within each layer, but all transactions in a given layer must complete before any in the next layer can begin.

To model the in-flow of money into the network, we introduce a special **source node**, which connects to all other nodes and distributes monthly incomes. To reflect a realistic distribution of funds, we use external data on mean and median salaries by age group, along with the population age distribution in Sweden [15]. Ages are represented as integers, and each account is assigned an age via inverse sampling from the empirical cumulative distribution function (CDF) shown in Fig. 2a. Given an assigned age, we retrieve the corresponding mean salary  $\mu_{\text{salary}}$  and median salary  $m_{\text{salary}}$  from [15], and model the income using a lognormal distribution:

$$p_{\text{salary}}(x) = \frac{1}{x\sigma_{\text{scale}}\sqrt{2\pi}} \exp\left(-\frac{(\log(x) - \mu_{\text{loc}})^2}{2\sigma_{\text{scale}}^2}\right),$$

with parameters defined as:

$$\mu_{\text{loc}} = \log(m_{\text{salary}}), \quad \sigma_{\text{scale}} = \sqrt{2 \log(\mu_{\text{salary}}) - \mu_{\text{loc}}}.$$

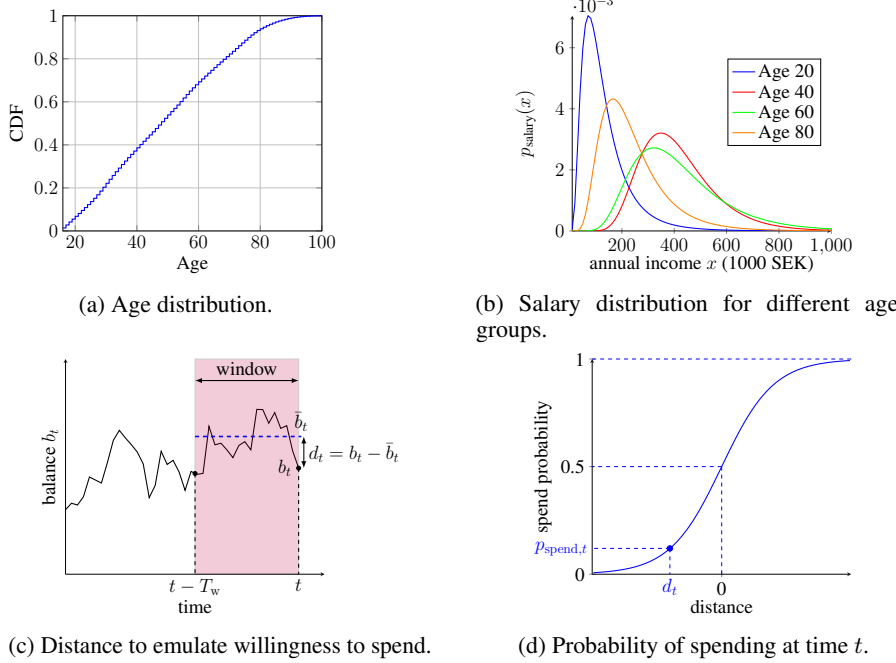


Figure 2: Components used to model in- and out-flow of the transaction network.

Fig. 2b shows the resulting distributions for selected ages 20, 40, 60, 80. The distribution shifts rightward with age, reflecting increasing income with seniority, and falls off around retirement age.

Analogous to the source node, we introduce a **sink node** to account for the out-flow of funds from the transaction network. The sink node acts as the recipient for all transactions that do not occur between two internal accounts, effectively modeling external spending. Spending behavior is simulated using a sliding window of length  $T_w$  to compute the average balance  $\bar{b}_t$  at time  $t$ . We then calculate the deviation from this average as  $d_t = b_t - \bar{b}_t$ , where  $b_t$  is the current balance. Intuitively, if  $d_t > 0$ , the account has a surplus relative to its recent history and is more likely to spend; if  $d_t < 0$ , spending is less likely. This is modeled probabilistically using a sigmoid function applied to  $d_t$ , yielding the spending probability at time  $t$ , denoted  $p_{\text{spend},t}$ . A transaction to the sink node occurs if a Bernoulli trial with success rate  $p_{\text{spend},t}$  returns one. The full process is illustrated in Fig. 2c and Fig. 2d.

All transactions in AMLGENTEX are associated with attributes  $a \in \mathcal{A}$ , including the transaction amount  $x$  and timestamp  $t$ . The amount is sampled from a truncated Gaussian distribution parameterized by a mean  $\mu$ , variance  $\sigma^2$ , a lower limit, and an upper limit. The lower limit is fixed to 1 SEK, representing the smallest possible transaction amount. For each agent, the upper limit is defined as the minimum of the current balance  $b_t$  and a maximum allowed amount  $x_{\max}$ . To distinguish between benign and money laundering transactions, amounts are sampled from separate truncated Gaussian distributions. This allows the difference in transaction behavior to be tuned: for example, the signal strength can be increased by widening the gap between  $\mu_{\text{normal}}$  and  $\mu_{\text{alert}}$ , see Fig. 3.

AMLGENTEX models money laundering process, via **placement**, **layering**, and **integration**. Illicit funds can be introduced in two ways: through transfer or cash. In the transfer method, the initiating account receives extra funds along with its salary. These funds are visible to the bank and are used in laundering transactions (see Fig. 4a). In the cash method, the account receives untracked funds before the laundering pattern begins. These funds are stored in a separate cash balance that is not visible to the bank. The cash may originate from criminal activity or from a cooperating end account. Once laundering begins, the cash is used while the bank balance remains unchanged (see Fig. 4b). To

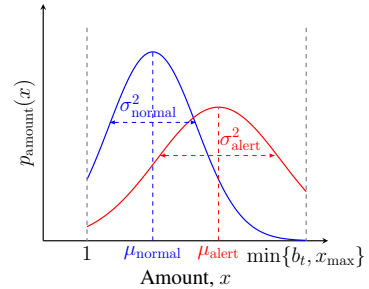
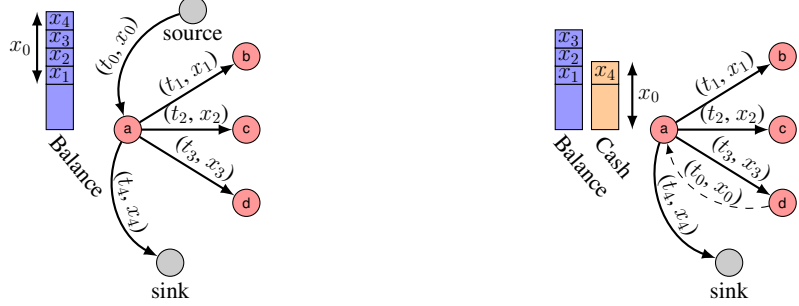


Figure 3: Transaction amount PDFs for a given account at time  $t$ : normal (blue) vs. laundering (red).



(a) **Placement:** At  $t_0$ , the source transfers  $x_0$  to account a. **Layering:** Account a sends  $x_1, x_2$ , and  $x_3$  to b, c, and d, keeping the remainder. **Integration:** At  $t_4$ , a spends  $x_4$  by sending it to the sink. (b) **Placement:** At  $t_0$ , account d sends cash  $x_0$  to a, invisible to the bank. **Layering:** a sends  $x_1, x_2, x_3$  to b, c, and d, retaining the rest. **Integration:** At  $t_4$ , a sends  $x_4$  to the sink.

Figure 4: Placement, layering, and integration in the different money-laundering procedures.

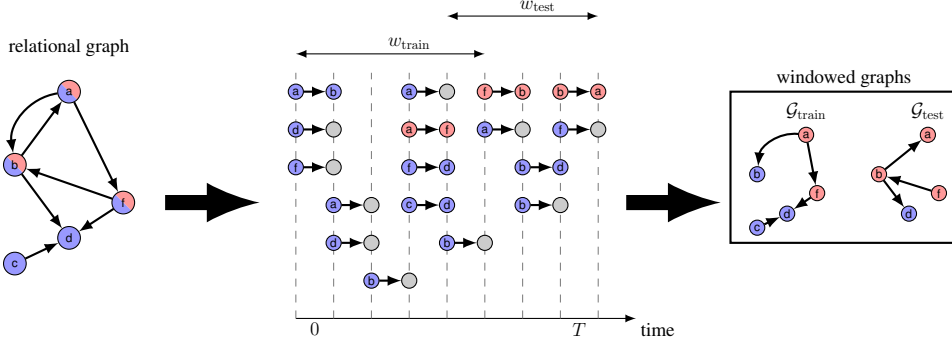


Figure 5: From the relational graph (left), transactions are generated over discrete time-steps. Transactions within the training and testing periods (center) are used to compute account features. The resulting transaction networks are shown on the right with sink transactions omitted.

reflect real world behavior, the laundering account keeps only a fraction of the received funds [18]. During integration, the account may choose to spend either from cash or from its bank balance. This is modeled as a Bernoulli trial with user defined probability, typically set high due to the decline of cash usage [19]. This behavior may create a weak signal for the FI, as the account's balance remains idle while cash is being spent.

### 4.3 Feature Engineering: Processing the Transaction Log

After generating the transaction data, a feature processing step is applied to prepare the data for machine learning. Let  $t = 0$  and  $t = T$  denote the start and end of the transaction log. To support both traditional monitoring approaches (e.g., decision trees) and graph-based methods, the transaction log is split into two user-specified time-windowed graphs: a training graph and a test graph. The training graph is constructed as  $\mathcal{G}_{train} \leftarrow \text{AGG}(w_{train})$ , where  $\text{AGG}$  aggregates transactions over the window  $w_{train}$ . A validation set is obtained by holding out a subset of nodes from  $\mathcal{G}_{train}$ . Similarly, the test graph is constructed as  $\mathcal{G}_{test} \leftarrow \text{AGG}(w_{test})$ , where  $w_{test}$  may overlap with  $w_{train}$ . This setup is illustrated in Fig. 5. Note that the train and test graphs can also be used with traditional methods by discarding the edges and treating nodes as independent instances.

The node features generated by the aggregation function are listed in Table 1 of App. C, and can be easily extended or modified. To avoid overfitting to the specifics of the data generation process, the feature design is inspired by [6, Sec. 8.2] and [18]. To enable fine-grained temporal analysis, the time period is divided into  $m$  sub-windows, and each feature is computed separately within each sub-window. As a result, even if an account appears in both  $\mathcal{G}_{train}$  and  $\mathcal{G}_{test}$ , its feature representation will likely differ. In addition, as shown in App. D, AMLGENTEX supports injecting label noise to reflect the uncertainty and biases inherent in the labeling process used by FIs.

AMLGENTEX also enables the creation of multiple local transaction networks, each representing a distinct financial institution (FI). This supports the evaluation of local, centralized, and federated

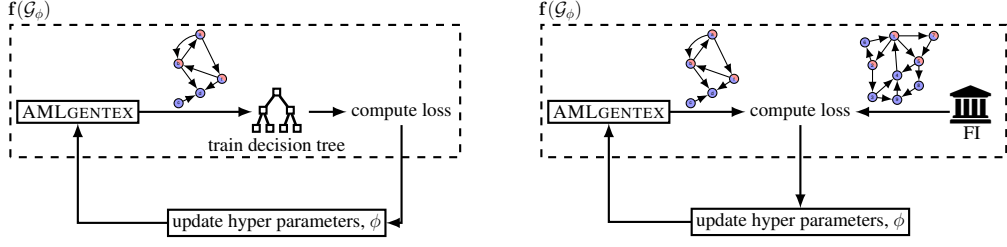


Figure 6: Optimization framework in the knowledge-free setting (a) and data-informed setting (b).

learning scenarios. Importantly, feature vectors are computed using only the information available to each FI. Thus, in local and federated settings, features are derived from the local view of the network, whereas centralized training can leverage global information.

## 5 Hyperparameter Tuning

AMLGENTEX requires the specification of several hyperparameters to generate synthetic transaction data. Setting these parameters is inherently challenging, as many are not publicly disclosed; revealing them could aid money launderers in mimicking benign behavior and evading detection. To address this, we offer two systematic approaches for parameter selection: (i) a knowledge-free setting, where no prior information on money laundering behavior is assumed, and (ii) a data-informed setting, where real transaction data is available for calibration. The first approach is suited for generating open access datasets, while the second is intended for use by FIs with access to sensitive data.

For both settings, our automatic parameter selection relies on multi-objective Bayesian optimization. We define a vector-valued objective function  $\mathbf{f}(\mathcal{G}_\phi) \in \mathbb{R}^k$ , where  $\mathcal{G}_\phi$  is the generated transaction graph parametrized by the hyperparameters  $\phi \in \Phi$  with  $\Phi$  denoting the space of available hyperparameters. Since the objectives may be conflicting, the goal is to approximate the Pareto-optimal set

$$\Phi^* = \{\phi \in \Phi \mid \nexists \phi' \in \Phi, \phi' \neq \phi : \mathbf{f}(\mathcal{G}_{\phi'}) \prec \mathbf{f}(\mathcal{G}_\phi)\},$$

where  $\mathbf{f}(\mathcal{G}_{\phi'}) \prec \mathbf{f}(\mathcal{G}_\phi)$  indicates that  $\mathbf{f}(\mathcal{G}_{\phi'})$  Pareto-dominates  $\mathbf{f}(\mathcal{G}_\phi)$ , i.e.,  $\mathbf{f}(\mathcal{G}_{\phi'})$  is no worse in all objectives and strictly better in at least one. Optimization is performed using BOHB [20], which combines Bayesian and bandit strategies, and is implemented via OPTUNA [21], which provides native support for multi-objective optimization.

In the *knowledge-free setting*, parameter selection must rely on publicly available information. For benign transactions in AMLGENTEX, we use aggregate statistics from Swish [16], a mobile payment system, such as the average number of transactions per account and the average transaction amount. Defining parameters for money laundering behavior is more challenging. To address this, we apply the optimization framework described above. We draw inspiration from publicly reported false positive rates (FPR) in rule-based AML systems, which are often as high as 90–98% [22, 23]. Let  $\mathcal{D}_\phi$  denote the individual node features in  $\mathcal{G}_\phi$  and let  $\text{FPR}(\mathcal{D}_\phi)$  denote the FPR of a decision tree trained on  $\mathcal{D}_\phi$ , with hyperparameters optimized using OPTUNA. Our first objective minimizes the deviation from an FPR target  $\text{FPR}_{\text{target}}$  as

$$f_1(\phi) = |\text{FPR}(\mathcal{D}_\phi) - \text{FPR}_{\text{target}}|.$$

To discourage reliance on individual features, we define a second objective promoting uniform Gini-based feature importance. Let  $\psi_i(\mathcal{D}_\phi)$  be the importance of feature  $i \in [N]$ , and let  $\bar{\psi}(\mathcal{D}_\phi)$  denote the mean importance. The second objective is defined as

$$f_2(\phi) = \sum_{i=1}^N |\psi_i(\mathcal{D}_\phi) - \bar{\psi}(\mathcal{D}_\phi)|.$$

Finally, we choose  $\phi \in \Phi^*$  closest to the FPR target. The process is illustrated in Fig. 6a.

In the *data-informed setting*, where real transaction data is available, a subset of the real transaction network,  $\mathcal{G}_{\text{target}}$ , can be used to calibrate the synthetic data by aligning key characteristics. These may include the degree distribution, average in- and out-degrees, and average transaction amounts. Given the sensitivity of such data, FIs can define custom objective functions and tolerances for acceptable similarity. This process is illustrated in Fig. 6b.

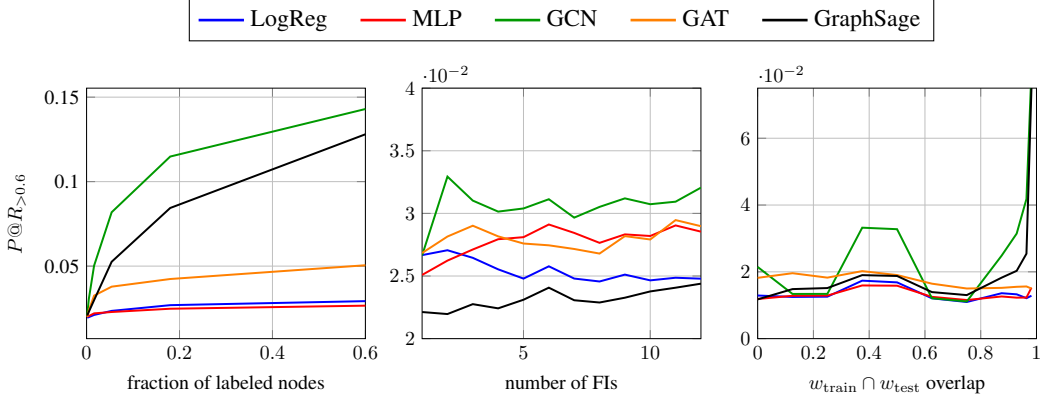


Figure 7: AML monitoring accounting for weak supervision (left), collaborative learning (center), and changing behavior (right).

## 6 Experiments

In this section, we evaluate the performance of traditional methods, including logistic regression and multilayer perceptron (MLP), as well as standard graph neural networks for node classification (GCN [24], GAT [25], and GraphSAGE [26]), to study the impact of the challenges outlined in Fig.1. The dataset (released at <https://huggingface.co/AMLGentex>), is generated using AMLGENTEX in a knowledge free setting, consists of 100,000 accounts uniformly distributed across 12 financial institutions over 112 time steps (16 weeks), and is configured with a target FPR of 98%. The data is highly imbalanced with only 1850 accounts being related to money laundering activities, see Fig. 15. The class homophily, measured as the proportion of neighbors sharing the same label, equals 0.98 and 0.52 for normal accounts and money launderers, respectively. Hence, most normal accounts connect to other normal accounts, while money laundering accounts are more mixed, suggesting attempts to blend in with normal activity. Detailed dataset statistics are provided in Appendix E.2 and details on hyper-parameters are provided in App. F. Given the importance of minimizing false negatives in AML settings, we report the average precision at recall values above 0.6 as the evaluation metric, denoted  $P@R_{>0.6}$ . For each model, results are further averaged over 10 independent seeds.

**Weak Supervision:** In this experiment, we study the impact of label scarcity in AML. We adopt a transductive setting where  $w_{\text{train}} = w_{\text{test}}$ , using features constructed from  $m = 4$  sub-windows of length 28. For each sub-window, we extract the features described in Appendix C and concatenate them to form the final representation. We assume a centralized setup where data from all financial institutions is available during training. As shown in Fig. 7 (left), performance declines as label availability decreases, with models varying in sensitivity. Notably, the graph-based methods GCN and GraphSAGE achieve the highest overall performance and benefit most from increased label access, while other models show only modest gains. Given the limited availability of labels in practice, it is crucial to develop models that remain effective under weak supervision.

**Privacy:** In this experiment, we consider the same setting as above but assume access to all node labels during training. We investigate the use of federated learning across the 12 FIs, employing Federated Averaging (FEDAVG)[27], with all FIs using identical hyperparameters as described in App.F. Fig. 7 (center) shows the performance of FEDAVG as more FIs join the federation. All models, except logistic regression, show a positive trend, i.e., it helps slightly to federate with more FIs. However, compared to the centralized setting, where accessing just 60% of the labels yields an average precision close to 0.15 the federated results suggest substantial room for improvement. One promising direction is to explicitly leverage inter-FI connections through subgraph federated learning [28, 29].

**Changed behavior:** In this section, we consider a scenario where money launderers employ three specific patterns during the first half of the simulated timeline, after which they switch to new typologies. Appendix E, Fig. 21, illustrates the number of transactions associated with each pattern that emerges in the data. We set  $w_{\text{train}} = \{1, \dots, 56\}$ , while the test window  $w_{\text{test}}$  is of the same length but varies in position. This setup effectively places us in an inductive setting, with a distribution

shift between the training and test graphs. For simplicity, we assume a centralized setting with access to node labels.

Fig. 7 (right) shows the test performance across different degrees of overlap between the training and test windows. As expected, larger overlap improves performance, since the test graph more closely resembles the training graph. Interestingly, the performance shows a nonmonotonic trend: it first declines as the test graph diverges from the training graph, but begins to improve again around 50% overlap. This effect is explained by the nature of the new patterns, specifically *scatter gather* and *gather scatter*, which contain *fan in* and *fan out* substructures at the start of their sequences (see Appendix A). Furthermore, as shown in Fig. 21, these new patterns account for significantly more transactions. Consequently, the early stage fan in and fan out components of the new patterns become discriminative, temporarily boosting performance. However, as the latter parts of the typologies dominate, the node representations diverge from the original patterns, leading to another performance drop.

## 7 Conclusion

AMLGENTEX offers a simulation suite for generating standardized AML benchmarks, enabling evaluation against a consistent baseline rather than relying on proprietary or limited public datasets. Its configurable simulation engine supports alignment with real world data and targeted method development. In our experiments, we use the framework to assess model robustness to missing labels and temporal drift, and to quantify gains from collaborative detection. Such analyses, grounded in realistic AML scenarios, can guide financial institutions in prioritizing investments—for example, when advanced graph based methods are appropriate or how missing labels affect detection performance. Moreover, empirical evidence of collaborative benefits can inform regulatory discussions and support public and private pilots by providing a neutral testbed for refining data sharing protocols.

**Limitations:** While the framework incorporates a detailed simulation mechanism, it cannot fully capture the complexity of real-world AML operations. Modeling known patterns such as fan-in and fan-out offers a useful approximation, but actual laundering schemes are often more diverse and sophisticated. Moreover, the simulation lacks differentiation between FIs in terms of customer profiles, KYC practices, and product constraints, limiting its reflection of real-world heterogeneity. Lastly, although AMLGENTEX allows some parameter-based adversarial adaptation, it does not model a dynamic feedback loop where criminals learn from detection and adjust their behavior accordingly.

**Ethical considerations:** Releasing a simulation suite for money laundering data raises legitimate ethical concerns, particularly whether its potential to advance AML research outweighs the risk of misuse. A key question is whether AMLGENTEX could equip criminals with tools to improve their evasion strategies. Importantly, the simulation framework introduces no novel insights into money laundering tactics: typologies, feature sets, and layering strategies are all drawn from documented criminal behavior and prior literature.

The primary theoretical risk lies in enabling adversaries to experiment with data-driven laundering strategies. In practice, however, we consider this risk minimal. The effectiveness of such experimentation is constrained by: (i) the opacity of institutional detection systems, which precludes replication or benchmarking; (ii) the limited fidelity of simulated environments relative to real-world transactional complexity; and (iii) unobservable factors such as labeling practices, risk thresholds, and customer demographics that critically influence detection outcomes. These factors are largely inaccessible to malicious actors and beyond their control. Furthermore, as detection systems grow more diverse and adaptive, adversarial anticipation becomes increasingly infeasible. We view AMLGENTEX as contributing to this trend.

The datasets released do not reflect the customer base of any particular FI. Instead, they are designed with expert input to support benchmarking and method development. We consider benchmarking an essential mechanism for collaboration and progress in AML research. As synthetic datasets begin to approximate real-world data more closely, future releases will require careful governance, and public availability may need to be restricted to trusted collaborators under appropriate safeguards.

## References

- [1] Kevin Sullivan. *Anti-money laundering in a nutshell: Awareness and compliance for financial personnel and business managers*. Springer, 2015.
- [2] Europol. The other side of the coin: Analysis of financial and economic crime, 2023. URL [https://www.europol.europa.eu/cms/sites/default/files/documents/The%20Other%20Side%20of%20the%20Coin%20-%20Analysis%20of%20Financial%20and%20Economic%20Crime%20\(EN\).pdf](https://www.europol.europa.eu/cms/sites/default/files/documents/The%20Other%20Side%20of%20the%20Coin%20-%20Analysis%20of%20Financial%20and%20Economic%20Crime%20(EN).pdf). Accessed: 2025-05-16.
- [3] Nasdaq Verafin. 2024 global financial crime report. Technical report, Nasdaq Verafin, 2024. URL <https://nd.nasdaq.com/rs/303-QKM-463/images/2024-Global-Financial-Crime-Report-Nasdaq-Verafin-20240119.pdf>. Accessed: 2025-05-15.
- [4] United Nations Office on Drugs and Crime (UNODC). Estimating illicit financial flows resulting from drug trafficking and other transnational organized crimes. Technical report, United Nations Office on Drugs and Crime, 2011. URL [https://www.unodc.org/documents/data-and-analysis/Studies/Illicit\\_financial\\_flows\\_2011\\_web.pdf](https://www.unodc.org/documents/data-and-analysis/Studies/Illicit_financial_flows_2011_web.pdf). Accessed: 2025-01-09.
- [5] Financial Action Task Force (FATF). International standards on combating money laundering and the financing of terrorism & proliferation: The fatf recommendations, 2012. URL <https://www.fatf-gafi.org/content/dam/fatf-gafi/recommendations/FATF%20Recommendations%202012.pdf.coredownload.inline.pdf>. Accessed: 2025-01-16.
- [6] Project aurora. Technical report, Bank for International Settlements, 2023. URL <https://www.bis.org/publ/othp66.pdf>. Accessed: 2025-05-15.
- [7] Ronald F Pol. Anti-money laundering: The world's least effective policy experiment? together, we can fix it. *Policy design and practice*, 3(1), 2020.
- [8] Europol. Eu serious and organised crime threat assessment (eu socta). <https://www.europol.europa.eu/cms/sites/default/files/documents/EU-SOCTA-2025.pdf>, 2025. Accessed: 2025-05-15.
- [9] Edgar Alonso Lopez-Rojas and Stefan Axelsson. Multi agent based simulation (mabs) of financial transactions for anti money laundering (aml). In *Nordic Conference on Secure IT Systems*, 2012.
- [10] Edgar Lopez-Rojas, Ahmad Elmira, and Stefan Axelsson. Paysim: A financial mobile money simulator for fraud detection. In *European Modeling and Simulation Symposium (EMSS)*, 2016.
- [11] Toyotaro Suzumura and Hiroki Kanezashi. Anti-Money Laundering Datasets: InPlusLab anti-money laundering datadatasets. <http://github.com/IBM/AMLSim/>, 2021.
- [12] Berkan Oztas, Deniz Cetinkaya, Festus Adedoyin, Marcin Budka, Huseyin Dogan, and Gokhan Aksu. Enhancing anti-money laundering: Development of a synthetic transaction monitoring dataset. In *IEEE International Conference on e-Business Engineering (ICEBE)*, 2023.
- [13] Erik Altman, Jovan Blanuša, Luc von Niederhäusern, Beni Egressy, Andreea Anghel, and Kubilay Atasu. Realistic synthetic financial transactions for anti-money laundering models. In *Neurips*, volume 36, 2023.
- [14] Rasmus Ingemann Tuffveson Jensen, Joras Ferwerda, Kristian Sand Jørgensen, Erik Rathje Jensen, Martin Borg, Morten Persson Krogh, Jonas Brunholm Jensen, and Alexandros Iosifidis. A synthetic data set to benchmark anti-money laundering methods. *Scientific data*, 10(1), 2023.
- [15] Statistics Sweden. Income Statistics for Individuals. <https://www.scb.se/hitta-statistik/sverige-i-siffror/utbildning-jobb-och-pengar/inkomster-for-personer/>, 2024. Accessed: 2025-05-15.
- [16] Swish. Swish Statistics and Downtime - January 2023. [https://assets.ctfassets.net/zrqoyh8r449h/6oxN3fzsfWDIsyVe00kAun/a5278f4f5ca783b25a0af2edbe15f043/Swish\\_statistics\\_\\_\\_downtime\\_january.pdf](https://assets.ctfassets.net/zrqoyh8r449h/6oxN3fzsfWDIsyVe00kAun/a5278f4f5ca783b25a0af2edbe15f043/Swish_statistics___downtime_january.pdf), 2023. Accessed: 2025-05-15.

[17] Kimmo Soramäki, Morten L Bech, Jeffrey Arnold, Robert J Glass, and Walter E Beyeler. The topology of interbank payment flows. *Physica A: Statistical Mechanics and its Applications*, 379(1), 2007.

[18] Finanspolisen. Finanspolisen informerar: Swish och penningvätt, 2018. URL <https://polisen.se/siteassets/dokument/finanspolisen/finanspolisen-informerar/fipo-informationsblad-swish.pdf>. Accessed: 2025-05-15.

[19] Sveriges Riksbank. Payments report, 2024. URL <https://www.riksbank.se/globalassets/media/rapporter/betalningsrapport/2024/engelsk/payments-report-2024.pdf>. Accessed: 2025-05-15.

[20] Stefan Falkner, Aaron Klein, and Frank Hutter. BOHB: Robust and efficient hyperparameter optimization at scale. In *ICML*, volume 80, 2018.

[21] Takuya Akiba, Shotaro Sano, Toshihiko Yanase, Takeru Ohta, and Masanori Koyama. Optuna: A next-generation hyperparameter optimization framework. In *ACM SIGKDD International Conference on Knowledge Discovery & Data Mining*, 2019.

[22] PwC US. Aml transaction monitoring systems: Understanding and mitigating risks. Technical report, PricewaterhouseCoopers (PwC), 2010. URL <https://www.pwc.com/us/en/anti-money-laundering/publications/assets/aml-monitoring-system-risks.pdf>. Accessed: 2024-10-26.

[23] McKinsey & Company. Transforming approaches to aml and financial crime, 2020. URL <https://www.mckinsey.com/~/media/mckinsey/business%20functions/risk/our%20insights/transforming%20approaches%20to%20aml%20and%20financial%20crime/transforming-approaches-to-aml-and-financial%20crime-vf.pdf>. Accessed: 2025-05-15.

[24] Thomas N Kipf and Max Welling. Semi-supervised classification with graph convolutional networks. In *ICLR*, 2017.

[25] Petar Veličković, Guillem Cucurull, Arantxa Casanova, Adriana Romero, Pietro Liò, and Yoshua Bengio. Graph attention networks. In *ICLR*, 2018.

[26] Will Hamilton, Zhitao Ying, and Jure Leskovec. Inductive representation learning on large graphs. *Neurips*, 30, 2017.

[27] Brendan McMahan, Eider Moore, Daniel Ramage, Seth Hampson, and Blaise Aguera y Arcas. Communication-efficient learning of deep networks from decentralized data. In *AISTATS*, 2017.

[28] Ke Zhang, Carl Yang, Xiaoxiao Li, Lichao Sun, and Siu Ming Yiu. Subgraph federated learning with missing neighbor generation. *Neurips*, 34, 2021.

[29] Javad Aliakbari, Johan Östman, and Alexandre Graell i Amat. Fedstruct: Federated decoupled learning over interconnected graphs. In *ICLR*, 2025.

[30] Financial Intelligence Unit (FIU) Swedish Police Authority. Annual report 2020, financial intelligence unit, 2020. URL [https://polisen.se/siteassets/dokument/polisens-arsredovisning/fipos-arsrapport/bq\\_pol039\\_arsrapport\\_finanspolisen\\_2020\\_eng\\_ta\\_pf.pdf](https://polisen.se/siteassets/dokument/polisens-arsredovisning/fipos-arsrapport/bq_pol039_arsrapport_finanspolisen_2020_eng_ta_pf.pdf). Accessed: 2025-05-15.

[31] Zhi-Hua Zhou. A brief introduction to weakly supervised learning. *National science review*, 5(1), 2018.

[32] PwC Luxembourg. Pwc luxembourg AML survey 2024: Key insights and trends in financial crime, 2024. URL <https://www.pwc.lu/en/financial-crime/anti-money-laundering/aml-survey-2024.html>. Accessed: 2025-05-15.

## A Typologies

The normal typologies available are shown in Fig. 8 and the available money laundering are shown in Fig. 9. The fan-in, fan-out, cycle, scatter-gather, gather-scatter, and stacked bipartite patterns can be of arbitrary size set by the user. Moreover, each typology is related to a timing schema chosen by the user.

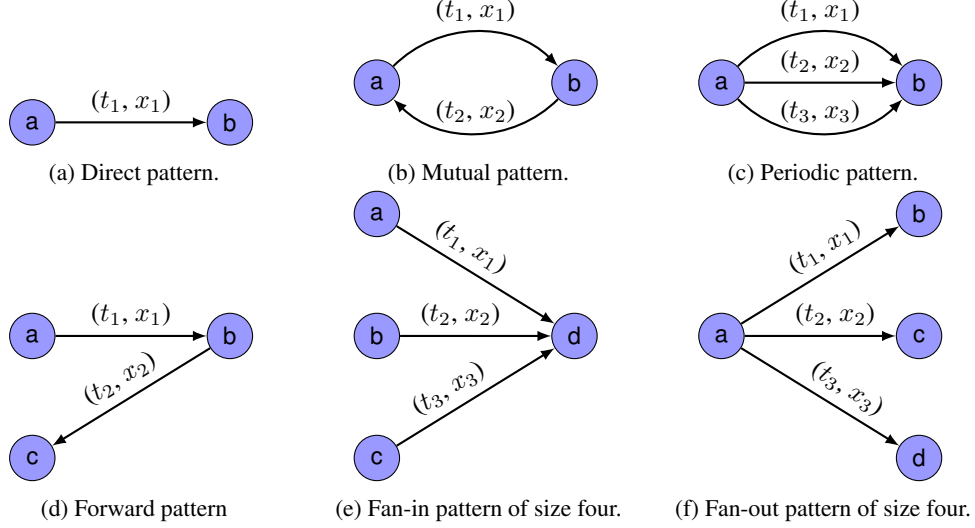


Figure 8: Normal patterns. Each transaction is associated with a time stamp  $t$  and an amount  $x$ .

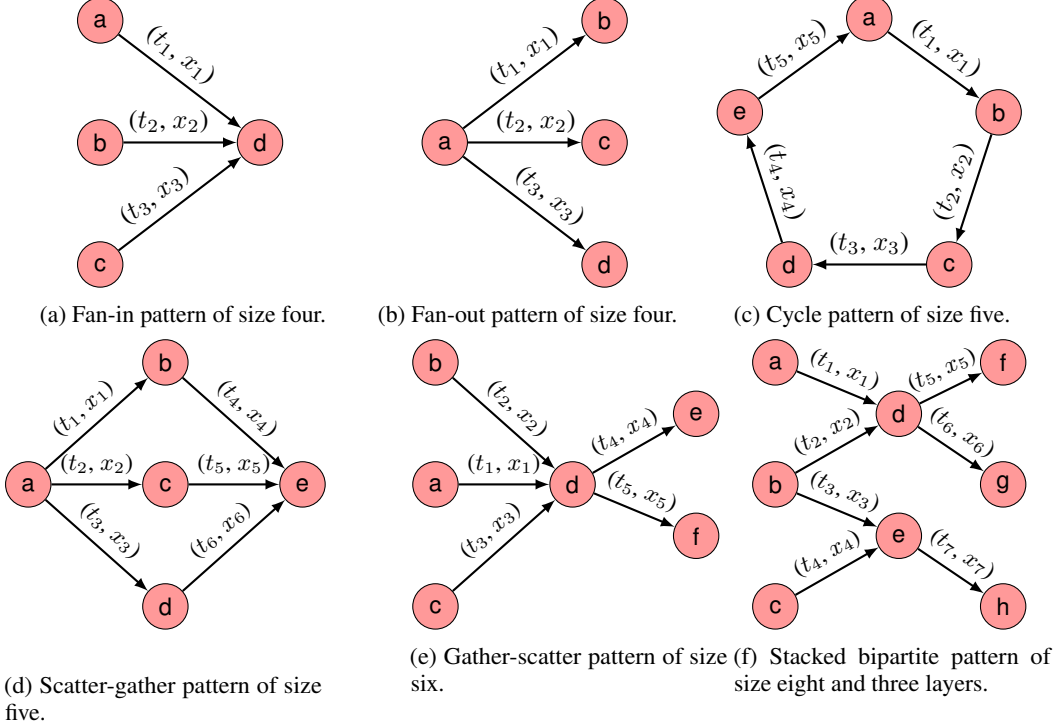


Figure 9: Laundering patterns. Each transaction is associated with time stamp  $t$  and an amount  $x$ .

## B Account Relations

The degree distribution of the blueprint network is controlled via a discretized Pareto distribution, parametrized by a triplet  $(\text{loc}, \text{scale}, \gamma)$ . In Fig. 10, the impact of the parameters are shown. Similarly, the probability of an account engaging in multiple money laundering patterns is given by a logarithmic distribution parameterized on  $p$  whose impact is shown in Fig. 11.

The complete process of defining a degree distribution, mapping it to a blueprint network, defining normal patterns and money laundering patterns, and fitting them into the blueprint network is illustrated in Fig. 12.

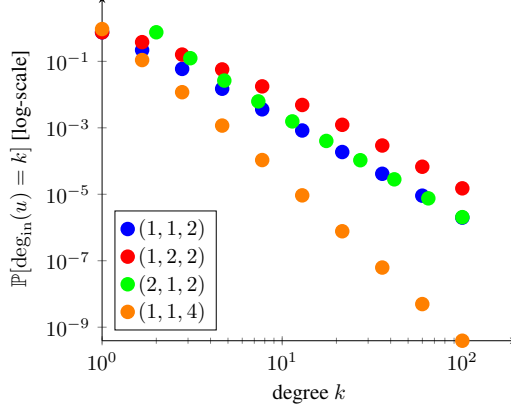


Figure 10: In-degree distribution for different values of  $(\text{loc}, \text{scale}, \gamma)$ .

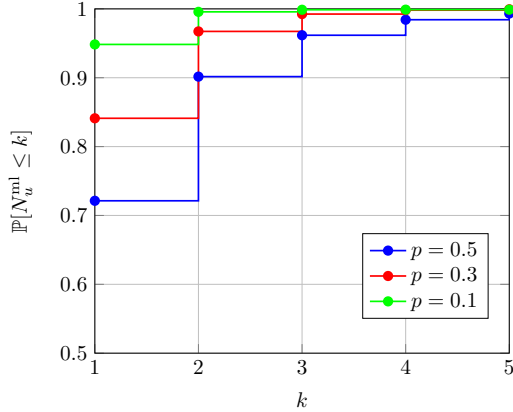
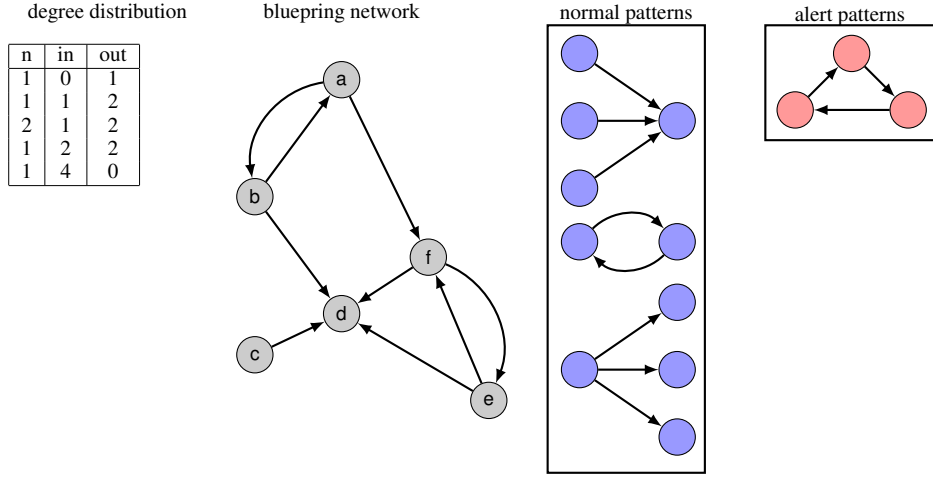
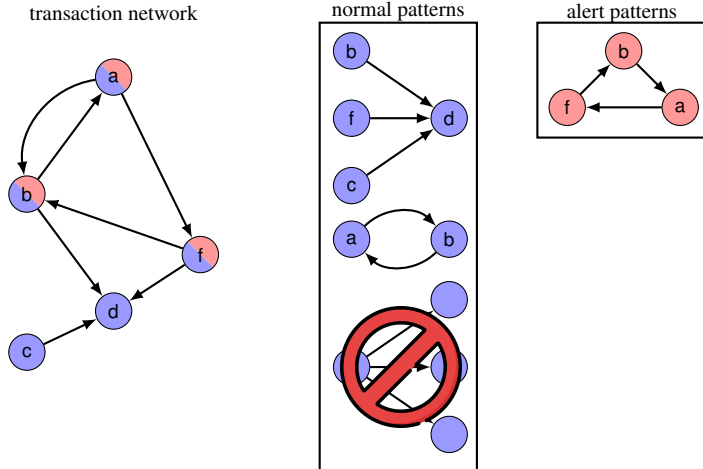


Figure 11: Logarithmic distribution modeling the number of money laundering events illicit accounts engage in.



(a) **Preparation of the Transaction Network:** A blueprint network is generated based on the degree distribution. User-defined normal patterns and alert patterns are then created for injection into the blueprint network. In the example above, the normal patterns consist of a fan-in pattern, a mutual pattern, and a fan-out pattern, while the alert pattern is represented by a cycle.



(b) **Pattern injection into the transaction network:** the simulator attempts to locate positions within the blueprint network that can accommodate normal patterns. If no suitable location is found for a given normal pattern, it is discarded and not included in the network. For example, in the case above, the fan-in pattern is mapped to nodes a, b, c, d, while the mutual pattern is mapped to nodes a, b. However, the fan-out pattern is discarded because no account has three outgoing transactions. In contrast, alert patterns are always inserted by randomly selecting nodes according to the distribution in Fig. 11. Specifically, for each node, it is first determined whether a node already involved in illicit transactions should be selected, or if a new node should be sampled uniformly at random from the entire graph. In the example above, nodes a, b, f are chosen for the alert pattern. Since there is no existing link between nodes f and b, a new link will be added to the graph. Additionally, as node e is not involved in any pattern, it will be pruned from the network. In the transaction network above, nodes that belong only to normal or alert patterns are represented as and , respectively, while nodes that belong to both normal and alert patterns are depicted as .

Figure 12: Preparation of the transaction network by generating a blueprint based on the degree distribution, followed by the injection of normal patterns (fan-in, mutual, and fan-out) and alert patterns (cycle) into the network. The simulator attempts to fit the normal patterns into suitable nodes, discarding those that cannot be placed, while alert patterns are randomly inserted, creating links between previously unconnected nodes as needed.

## C Feature Engineering

To create the training and test graph, the transaction network is windowed over  $w_{\text{train}}$  and  $w_{\text{test}}$ . Within each window, multiple subwindows are used to collect the transactions within the subwindow and computing the features in Table 1. Notably, these features are inspired by [6, 30]. Once the features for each subwindow has been obtained, they are concatenated to create the feature vector of the corresponding train/test graph.

Table 1: Features created for an account based on its transaction history over a time period.

Metric	Description
sum_spending	Total amount spent by an account.
mean_spending	Average amount spent by an account.
median_spending	Median amount spent by an account.
std_spending	Standard deviation of amounts spent by an account.
max_spending	Maximum amount spent in a single transaction.
min_spending	Minimum amount spent in a single transaction.
count_spending	Total number of outgoing transactions.
sum	Total transaction amount for an account.
mean	Average transaction amount for an account.
median	Median transaction amount for an account.
std	Standard deviation of transaction amounts.
max	Maximum transaction amount for an account.
min	Minimum transaction amount for an account.
count_in	Number of incoming transactions.
count_out	Number of outgoing transactions.
count_unique_in	Number of unique counterparties sending transactions.
count_unique_out	Number of unique counterparties receiving transactions.
count_days_in_bank	Number of days an account has been active.
count_phone_changes	Number of phone number changes for an account.

## D Data Impurities

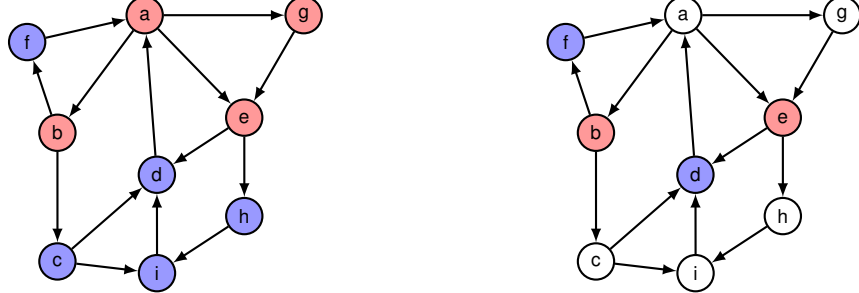
Following the creation of  $\mathcal{G}_{\text{train}}$  and  $\mathcal{G}_{\text{test}}$  from Section 4.3, we introduce a method to create impurities in the data to better reflect reality. In particular, we adopt the view of weakly supervised learning [31], considering both incomplete labels and inaccurate labels. Unlike fully supervised learning, where each training instance is associated with a precise output label, weakly supervised learning tackles scenarios where acquiring high-quality labels is either expensive or impractical.

Let each account  $i$  be represented by a tuple  $(\mathbf{x}_i, y_i) \in \mathcal{X} \times \{0, 1\}$ , where  $\mathbf{x}_i$  is the feature vector of node  $i$ , constructed as outlined in Section 4.3,  $y_i$  is its binary label, and  $\mathcal{X} = \mathcal{X}_{\text{XCDD}} \times \mathcal{X}_{\text{XTXN}}$  denotes the feature space. Define  $\mathcal{D}_{\text{train}}$  as all the node information of  $\mathcal{G}_{\text{train}}$ , with index sets  $\mathcal{I}_{\text{labeled}}$ ,  $\mathcal{I}_{\text{unlabeled}}$ , and  $\mathcal{I}_{\text{inaccurate}}$  representing data points with ground truth labels, missing labels, and inaccurate labels, respectively. The training data is then given by

$$\mathcal{D}_{\text{train}} = \bigcup_{i \in \mathcal{I}_{\text{labeled}}} \{\mathbf{x}_i, y_i\} \cup \bigcup_{i \in \mathcal{I}_{\text{unlabeled}}} \{\mathbf{x}_i\} \cup \bigcup_{i \in \mathcal{I}_{\text{inaccurate}}} \{\mathbf{x}_i, \tilde{y}_i\}, \quad (1)$$

where  $\tilde{y}_i$  denotes an erroneous label for node  $i$ . Naturally, the supervised setting is recovered for  $\mathcal{I}_{\text{unlabeled}} = \mathcal{I}_{\text{inaccurate}} = \emptyset$ .

Transaction networks at FIs inherently contain a large number of unlabeled transactions and only a few labeled instances. This scarcity is primarily due to the high cost and complexity of labeling. Each labeled transaction must pass rigorous scrutiny from the FI's compliance teams, requiring in-depth investigations into transaction histories and cross-referencing multiple sources. Moreover, labels generated internally, such as those transactions reported to financial authorities, do not always indicate confirmed cases of money laundering. Even if a reported case proceeds to court and results in a conviction, which would confirm it as money laundering, feedback on these outcomes rarely reaches the FI promptly, if at all. This lack of timely feedback means that by the time FIs receive confirmation,



(a) Ground truth data consisting of a single illicit fan-out pattern including accounts {a, b, e, g}. (b) Accounts {a, c, g, h, i} do not have a label. (c) Class noise: benign account {h} and suspicious accounts {g, e} are mislabeled. (d) Typology noise: accounts belonging to a given pattern are mislabeled. Here, account {b} is falsely flagged as benign. (e) Neighbour noise: nodes in the vicinity of laundering accounts are mislabeled. Here, accounts {d, f} are flagged as suspicious because of their interactions with {a, b} and {a, f}, respectively.

Figure 13: Toy example illustrating the different types of label noise. Suspicious accounts are denoted as and benign nodes as . Moreover, mislabeled nodes are denoted by and nodes without a label are denoted by .

the patterns involved may already be outdated, as criminals continuously adapt their methods to evade detection. Additionally, privacy regulations restrict FIs from sharing flagged events with one another, limiting opportunities to aggregate and learn from each institution’s data. Consequently, labeling remains scarce, costly, and fragmented across the financial industry. In AMLGENTEX, the user may provide a fraction of labeled nodes whereafter the labels in the training data will be pruned accordingly and not used during the training, see Fig. 13b.

Current rule-based systems are known for a high false-positive rate. As investigators get fed with many false positives, it is possible that the transaction gets flagged simply out of caution, resulting in false positive labels for the training. Since this process is largely manual, there are also personal biases involved in the labeling. Moreover, due to the scarce feedback from regulatory authorities, the labels are difficult to verify. Also, as money launderers constantly adapt, it is possible that the monitoring system misses illicit transactions or that the investigator falsely closes a case, resulting in a false negative. In AMLGENTEX, this labeling noise is managed by introducing two types of perturbations: *class noise* and *typology noise*. These add controlled inaccuracies to the training graph,  $\mathcal{G}_{\text{train}}$ , where the user sets a flip probability for both benign and illicit accounts. Accounts are then randomly flipped according to these probabilities, introducing false positives and false negatives into the training data, as illustrated in Fig. 13c and Fig. 13d.

Since monitoring systems often flag accounts based on network analysis, accounts connected to high-risk entities may also be flagged due to guilt by association. To model this in AMLGENTEX, we introduce *neighbor noise*. As shown in Fig. 13e, accounts connected to known money laundering entities are randomly flagged based on a user-defined probability, simulating the impact of network-based flagging errors.

## E Experimental Data

In this section, we illustrate the generated dataset based on the method presented in 6a. The degree distribution, see Section B, is generated using  $\gamma = 2.0$ ,  $\text{loc} = 1.0$ , and  $\text{scale} = 1.0$ . We attempt to fit 80,000 instances of each normal pattern and allow sizes between three and ten for fan-in and fan-out patterns (the remaining patterns are fixed in size).

### E.1 Finding the Hyperparameters

To decide the parameters going into the dataset generation, we fix the parameters for the normal patterns as shown in the *Normal* column of Table 2 by using publicly available information from the Swish mobile payment system [16]. We then optimize the money laundering parameters, i.e., the mean and variance of the transaction size distribution, the probability of spending cash if available, the probability to participate in multiple alert patterns, and the parameters going into the phone and bank changes, respectively, by means of Bayesian optimization using OPTUNA. As an objective, we make use of the average precision for recall larger than 0.6, and target an FPR of 0.98 when forced to use a decision tree classifier. This value is chosen based on reported values from the literature and aims to create a dataset that is very challenging for classical methods, see, e.g., [32]. The resulting parameters for the money laundering patterns are shown in Table 2 under column *Money laundering*.

Table 2: Parameter values for transactions within different normal and alert typologies. The normal parameters are selected from [16] whereas the money laundering parameters are optimized.

Parameter	Normal	Money laundering
mean amount	637	799
standard deviation amount	300	163
max amount	150000	150000
min amount	1.0	1.0
mean outcome	500	328
mean phone change	1460	1272
standard deviation phone change	365	281
mean bank change	1460	1335
standard deviation bank change	365	368
probability of multiple alert patterns	-	0.218

To create the final transaction graphs, we employ the parameters in Table 2 and run the simulation for 112 time-steps corresponding to 16 weeks. We then let  $w_{\text{train}} = w_{\text{test}} = [0, 112]$ . That is, the training and test period overlap for all of the data. Hence, after creating the feature representations, the train and test graph contain the same nodes and edges but differ in the labels considered. To create the features, we consider  $m = 4$  sub-windows, each of size 28, and compute the values in Table 1 for each window.

### E.2 Data Statistics

In Fig. 14, we show the degree distribution of the dataset for FI 1 along with the estimated parameters in the Pareto distribution.

In Fig 15, the node (account) and edge count for the transaction network at each FI is displayed alongside the centralized setting (all). It can be seen that the the 98.15% of the accounts are benign whereas 99.72% of the transactions are benign. Hence, out of the 100000 accounts, only 1850 accounts engage in money laundering.

Focusing on the money laundering patterns, in Fig. 16, it can be seen that patterns occur across multiple FIs with some patterns spanning up to seven FIs. Moreover, it can be seen that the alert patterns vary in size ranging between 5 and 20 accounts, sometimes containing more than 40 transactions within the pattern.

Next, considering FI 1, Fig. 17 illustrates the empirical distributions of transaction amounts and the number of transactions for both normal and mony-laundering accounts. From the first row, we observe that the empirical distributions of transaction size and transaction count differ only slightly

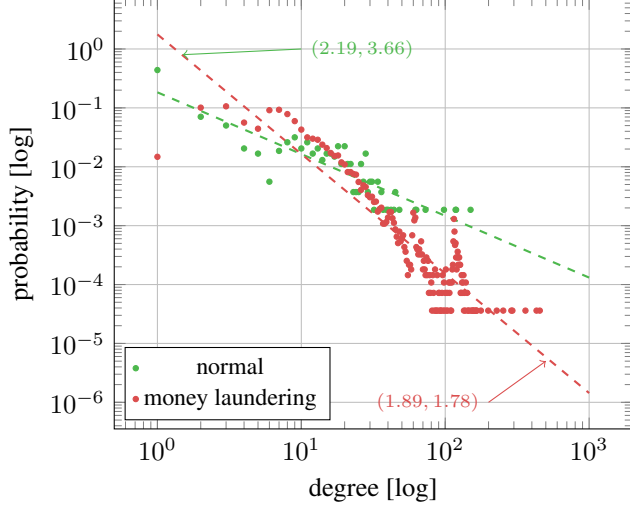


Figure 14: Degree distribution for FI A (left), FI B (middle) and FI C (right). The dashed lines correspond to fitted lines with parameters  $(\gamma, \text{scale})$  as shown in the figure.

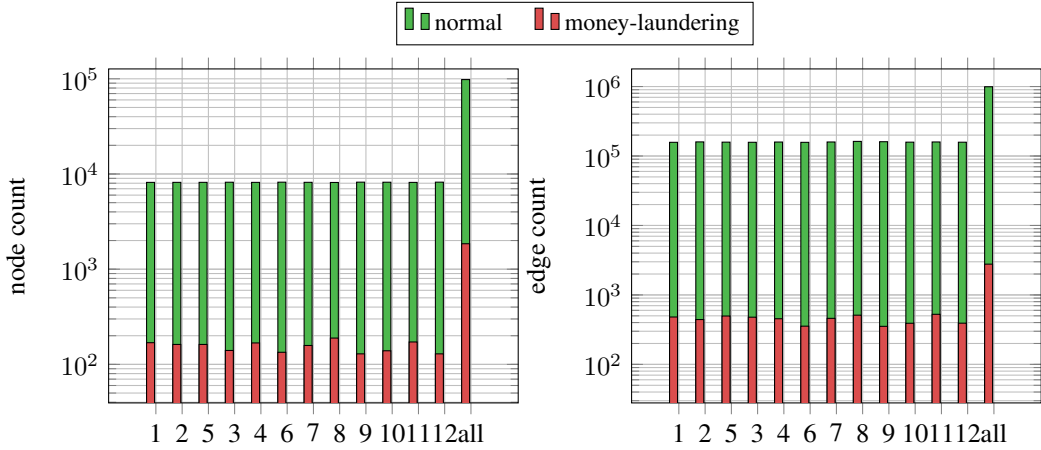


Figure 15: Node (left) and edge (right) counts of positive and negative labels for the generated datasets across FI 1 to FI 12.

between the negative and positive classes. However, the distributions for sink transactions (bottom row) appear similar. This suggests that transaction amount and transaction count contain some signal relevant to distinguishing between the two classes but a monitoring algorithm must look beyond.

The pattern counts for FI 1 are shown in Fig. 18 for the different datasets. It can be seen that the transaction network consists of a plethora of different typologies. In Fig. 20, we demonstrate three randomly chosen money laundering patterns and the transactions that accounts involved engage in. As can be seen, the patterns are of varying complexity and the money launderers involve also in normal transactions.

In Fig. 19, we illustrate some randomly sampled account balances from FI 1 for all time steps in the dataset. It can be seen that each account exhibits a highly individual behavior.

Finally, in Fig. 21, we illustrate the money laundering transactions related to our third experiment in Section 6 pertaining to changed behaviour. It can be seen that the money launderers engage in different typologies within the first and second half of the dataset.

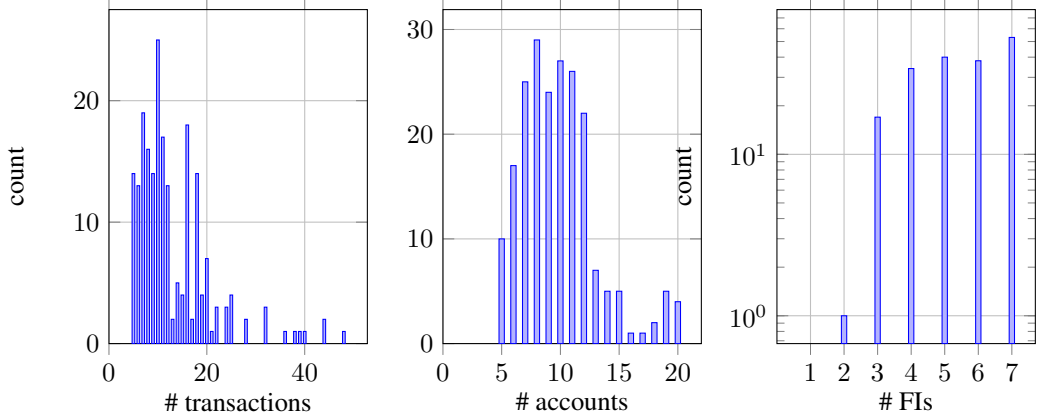


Figure 16: Overview of money laundering typologies in the global transaction graph. Specifically, the plots show: (left) the number of transactions associated with each typology, (middle) the number of accounts involved, and (right) the number of financial institutions spanned by each pattern.

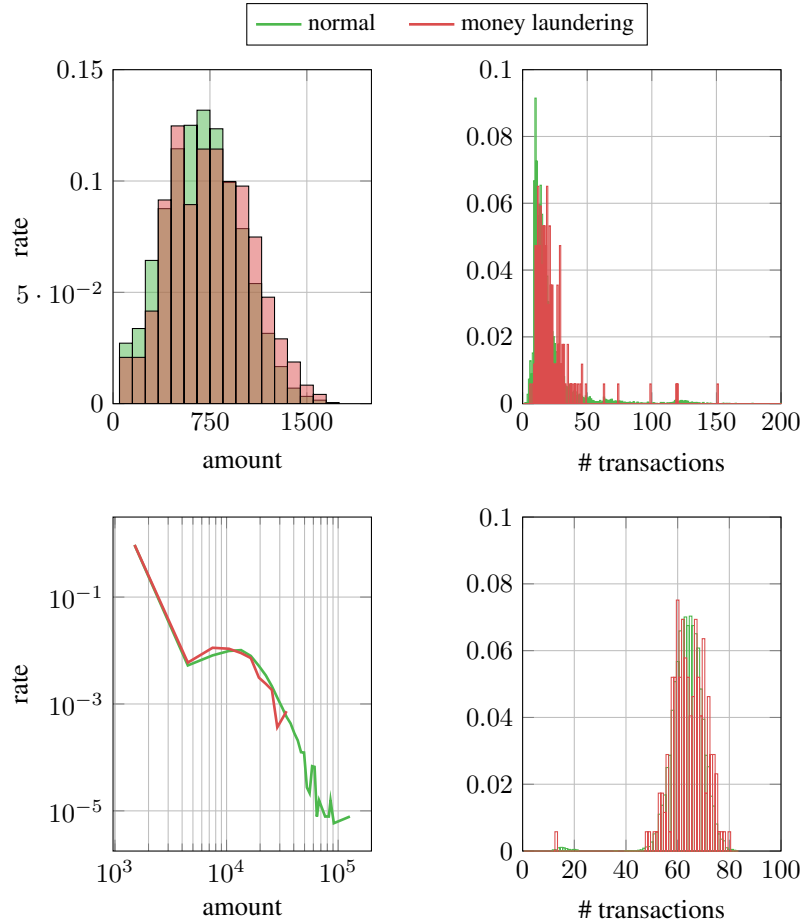


Figure 17: Empirical distributions within a single financial institution: (upper left) distribution of individual transaction amounts; (upper right) number of account-to-account transactions; (lower left) cumulative distribution of the total amount sent to the sink per account; and (lower right) number of transactions to the sink per account.

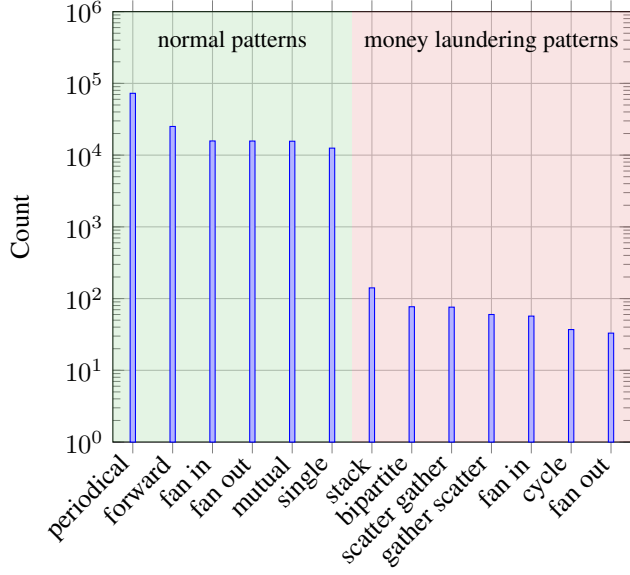


Figure 18: Different patterns in the local transaction network of FI A. Normal patterns are shown with a green background and alert patterns are shown with a red background. The count for all three datasets are included in the figure.

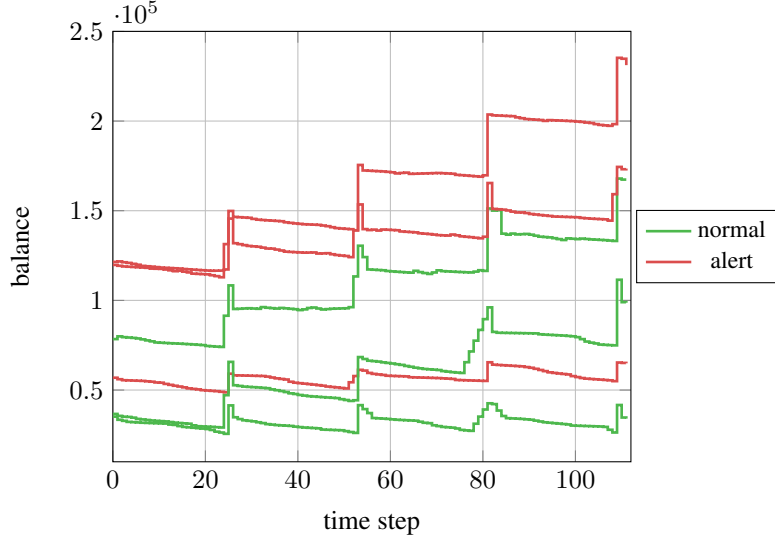


Figure 19: Account balances of three non-laundering accounts and three laundering accounts.

## F Model Parameters

For all experiments in Section 6, we use the same hyper parameters. In particular, we consider the transductive setting, i.e., the train and test graphs are the same. Assuming access to node-labels, we obtain the hyperparameters of each model by means of Bayesian optimization. The search space and obtained parameters for both the centralized and the federated settings are displayed in Table 3.

During model training, we employ the binary cross-entropy loss function, the ADAM optimizer, early stopping, a batch-size of 512 and train for 300 epochs.

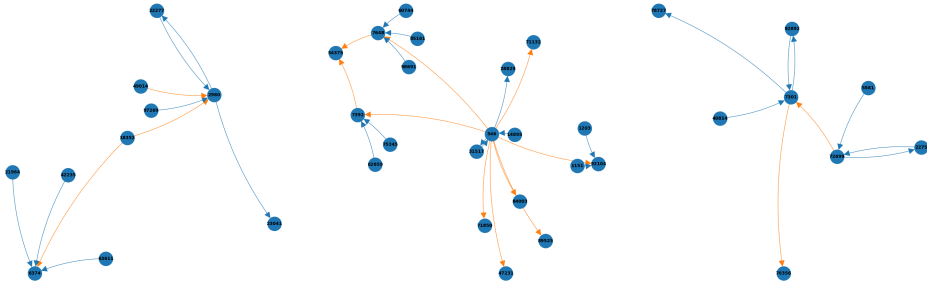


Figure 20: Example patterns from the dataset. Orange links refer to money laundering transactions and blue links refer to normal transactions.

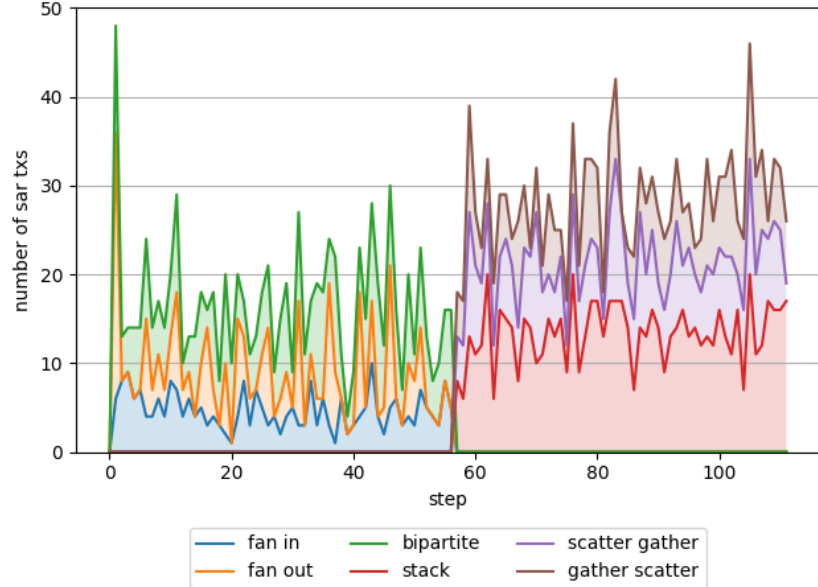


Figure 21: Prevalence of different money laundering transactions and what patterns they belong to. Within time steps 1 to 56, only fan-in, fan-out, and bipartite typologies are utilized. After step 56, the typologies are changed to stack, scatter-gather, and gather-scatter.

Table 3: Bayesian optimization search space and the obtained values.

model	parameter	search range	centralized	federated
GAT	dropout	[0.2, 0.9]	0.3449	0.2912
GAT	hidden dimension	[100, 300]	272	283
GAT	learning rate	[0.0001, 0.1]	0.0115	0.0617
GAT	layers	[1, 5]	4	1
GCN	dropout	[0.2, 0.9]	0.2125	0.2029
GCN	hidden dimension	[100, 300]	228	103
GCN	learning rate	[0.0001, 0.1]	0.0499	0.0543
GCN	layers	[1, 5]	2	1
GraphSAGE	dropout	[0.2, 0.9]	0.2075	0.3633
GraphSAGE	hidden dimension	[100, 300]	168	270
GraphSAGE	learning rate	[0.0001, 0.1]	0.0001	0.0011
GraphSAGE	layers	[1, 5]	5	1
LogisticRegressor	learning rate	$[10^{-5}, 0.01]$	0.0052	0.0100
MLP	hidden dimension	[50, 300]	294	259
MLP	learning rate	$[10^{-5}, 0.01]$	0.0000	0.0017
MLP	hidden layers s	[1, 5]	1	1
MLP	weight decay	[0.0, 1.0]	0.0044	0.0005